RESEARCH ARTICLE doi.org/10.1002/adsc.202300527

Dissymmetrically Substituted Diphosphines with Two Atropisomeric Axes and Their Application in Asymmetric Hydrogenation of Imines

Gaspard Hedouin,[a] Racha Abed Ali Abdine,[a] Quentin Dherbassy,[a] Christophe Michon,[a] Ignacio Funes-Ardoiz,[b,*] Françoise Colobert,[a] and Joanna Wencel-Delord[a,*]

[a] Laboratoire d'Innovation Moléculaire et Applications, ECPM, UMR 7042, Université de Strasbourg/Université de Haute-Alsace, 25 rue Becquerel, Cedex 67087, Strasbourg, France
E-mail: wenceldelord@unistra.fr
[b] Department of Chemistry, Centro de Investigación en Síntesis Química (CISQ), University of La Rioja, Logroño 26006, Spain
E-mail: ignacio.funesa@unirioja.es

Manuscript received: May 25, 2023; Version of record online: June 7, 2023

Supporting information for this article is available on the WWW under https://doi.org/10.1002/adsc.202300527

© 2023 The Authors. Advanced Synthesis & Catalysis published by Wiley-VCH GmbH. This is an open access article under the terms of the Creative Commons Attribution Non-Commercial NoDerivs License, which permits use and distribution in any medium, provided the original work is properly cited, the use is non-commercial and no modifications or adaptations are made.

Abstract: Despite the great potential and widespread applications, the majority of diphosphine ligands used in asymmetric catalysis are C_2-symmetric and their structural modifications are often limited. Herein, we reported the design of original enantiopure dissymmetrical diphosphines, BiaxPhos, bearing two atropisomeric axes. Their original chiral architecture combined with important modularity, renders BiaxPhos ligands appealing candidates for asymmetric catalysis, as illustrated by the Ir-BiaxPhos catalyzed asymmetric imines hydrogenation, furnishing chiral amines with excellent enantioselectivities under mild conditions. Remarkably, combined experimental mechanistic investigations and DFT calculations delineate yet unexplored mechanistic scenario implying the hydrogenation of the enamine tautomeric form instead of the classic reduction of the imine.

Keywords: Atropisomeric diphosphine; Dissymmetric ligand; Imine hydrogenation; Iridium; Mechanism

Introduction

Chirality is a unique feature of nature, that has been continuously inspiring chemists. Therefore, it is not surprising that the implementation of chiral information within the design of complex drugs, agrochemicals, and fragrances but also modern organic materials has been one of the key leverages to provide unique properties to the molecules of interest. While preparation of enantiopure molecules starting from a chiral pool or via chiral resolution of a racemic mixture has proven for decades to be a solution of choice for the large-scale assembly of enantiopure compounds, various limitations of these approaches make them incompatible with the sustainable chemistry mindset dominating recent progress in organic chemistry. Consequently, asymmetric synthesis allowing the direct synthesis of a desired enantiopure molecule with high optical purity has established itself as a methodology of choice not only in academia but progressively also in the industrial production of chiral products. In this context, various strategies including organocatalysis and enzymatic reactions have been investigated, but organometallic asymmetric catalysis remains arguably the most general and versatile approach.

The continuous expansion of the asymmetric organometallic chemistry requires perpetual design of advanced chiral ligands with improved reactivity, selectivity, and high modularity. Following the pioneering report by Kagan on the use of a diphosphine ligand (DIOP) for asymmetric hydrogenation of the 2-phenylacrylic acid, the development of phosphorus ligands

© 2023 The Authors. Advanced Synthesis & Catalysis published by Wiley-VCH GmbH

has become particularly attractive.[1] Therefore, diphosphines are, for the time being, among the most broadly applied and explored ligands in asymmetric catalysis.[2] During the past decades, a diversity of diphosphines has been conceived and among them, C_2-symmetric ligands with central, axial or planar chirality were the most extensively studied. However, despite their general applications, the modularity of their steric and electronic features remains frequently limited. On the other hand, the development of C_1-symmetric chiral diphosphines,[3] allowing independent and fine adjustment of the properties of each *P*-motif, is clearly underdeveloped due to their frequently tedious synthesis. Accordingly, C_1-symmetric diphosphines are mainly limited to ferrocenyl-derived diphosphines, including Josiphos,[4] Walphos[5] and derivatives.[6] From the conceptual viewpoint, the design of diphosphine ligands with two distinct phosphine motifs is expected to offer a unique possibility to perfectly adjust steric and electronic properties of the ligand. In addition, such a ligand design should also be considered as a complementary handle to impart an additional level of dissimilarity around the metal, thus enhancing the enantiodiscrimination within a stereoselective reaction. Discovery of innovative enantiopure C_1-diphosphine scaffolds and their straightforward synthesis via the stepwise installation of two different phosphine units are thus extremely appealing, holding a promise of opening new perspectives in asymmetric catalysis (Scheme 1.A).

Following our interest in the Pd-catalyzed asymmetric C–H functionalization field, we have developed a synthesis of axially chiral biaryls via sulfoxide-directed C–H activation.[7] This methodology paved also the way towards new enantiopure scaffolds: *ortho*-terphenyls **1** bearing two atropisomeric axes.[8] Due to the possible straightforward modification of the sulfoxide and Br-substituents in a presence of lithium bases, this new chiral skeleton appears as an appealing platform for the conception of new chiral ligands. Indeed, a unique late-stage modification of this original enantiopure scaffold allows direct installation of various coordinating units, including diverse phosphine moieties, at the strategic positions. Accordingly, in our preliminary work,[8] simultaneous sulfoxide and bromine lithium exchanges followed by trapping with a phosphine electrophile furnished the very first BiaxPhos ligand exhibiting two identical phosphine motifs. However, valorization of **1** via synthesis of dissymmetrically substituted diphosphines BiaxPhos* presents an infinitely more delicate task as a fully chemoselective sulfoxide/Li and Br/Li exchange has yet to be reached.

Herein we report the synthesis of new C_1-symmetric and highly modulable diphosphines, BiaxPhos and BiaxPhos*. The importance of the fine adjustment of the steric and electronic properties of each of the coordinating *P*-motifs is illustrated on asymmetric iridium-catalyzed imine hydrogenation.[9] Perfectly tuned BiaxPhos and BiaxPhos* thus promote the formation of the desired amines with excellent chiral induction and under very mild reaction conditions. Remarkably, the original structure of these ligands seems also to impart unprecedented reactivity of the corresponding iridium-complex translating into unusual mechanistic scenario for this imine hydrogenation. Contrary to the commonly acknowledged imines hydrogenation mechanisms occurring either via inner- or outer-sphere route,[10] the experimental studies combined with detailed DFT calculations suggest that Ir-BiaxPhos complex promotes highly stereoselective enamine reduction. Accordingly, this study clearly expands the state-of-the-art comprehension of asymmetric imines hydrogenation (Scheme 1.B).

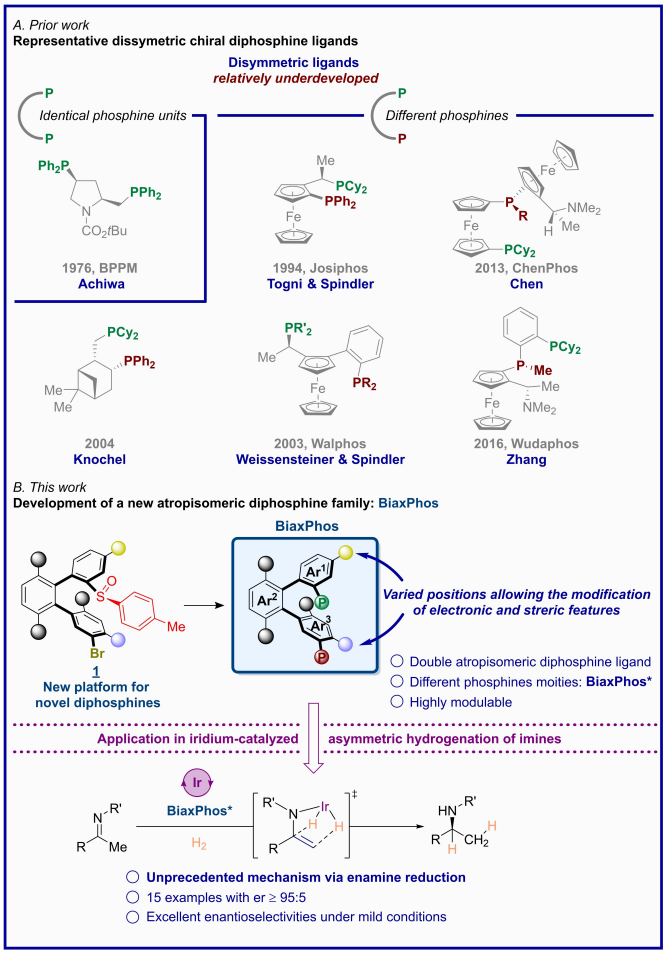

Scheme 1. (A). Examples of C_1 chiral diphosphines bearing two different phosphine motifs; (B) Development of new atropisomeric diphosphines and application as ligands in iridium-catalyzed asymmetric hydrogenation of imines.

© 2023 The Authors. Advanced Synthesis & Catalysis published by Wiley-VCH GmbH

16154169, 2023, 12, Downloaded from https://onlinelibrary.wiley.com/doi/10.1002/adsc.202300527 by Universidad de la Rioja, Wiley Online Library on [29/11/2023]. See the Terms and Conditions (https://onlinelibrary.wiley.com/terms-and-conditions) on Wiley Online Library for rules of use; OA articles are governed by the applicable Creative Commons License

Results and Discussion

Preparation of BiaxPhos ligands

To correlate the structure of the BiaxPhos ligands with their catalytic reactivity and chiral induction, the synthesis of a library of BiaxPhos ligands bearing both, two identical PAr_2 motifs as well as their BiaxPhos* congeners, featuring two different PAr_2 and PAr'_2 groups were targeted. The terphenyl scaffold **1** is the common precursor for both types of ligands and can be prepared by C–H directed arylation according to our previous work.[8] Indeed, the sulfoxide moiety, which serves as a directing group for the palladium-catalyzed C–H arylation during the construction of **1**, can be easily replaced by a variety of coordinating motifs[11] via sulfoxide lithium exchange[12] followed by electrophilic trapping. In particular, the introduction of the phosphine moiety should be possible while using $ClPAr_2$ as an electrophile. Moreover, the bromine substituent on *meta* position of Ar^3 allows the installation of the second phosphine moiety by halogen/lithium exchange. Accordingly, in the presence of a sufficiently strong lithium base, simultaneous lithiation of the two reactive sites should be possible, while quenching with an excess of the phosphine-type electrophile would deliver the "pseudo-symmetric" BiaxPhos ligands bearing two identical PAr_2 moieties (Scheme 2, Route A). However, although generally difficult to control, the relatively weak reactivity difference between the sulfoxide and the bromine with the lithium bases, hold a promise of exploring the second route. Indeed, a sequential lithiation and functionalization of the C-sulfoxide bond, followed by the C–Br motif is expected to pave the way towards "dissymmetrical introduction" of two distinguished phosphine units (Scheme 2, Route B). These two routes point out the high degree of tunability of this scaffold furnishing BiaxPhos and BiaxPhos* ligands via the late-stage modification of the complex chiral platform.

Following the first strategy (Route A), simultaneous sulfoxide/lithium and bromine/lithium exchanges occurred smoothly when the substrate **1a** was reacted with 5 equivalents of *t*-butyllithium at −94 °C (Scheme 3). The excess of *t*-BuLi is essential to generate the desired dilithiated intermediate in full

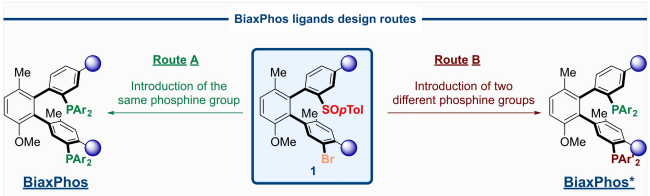

Scheme 2. Strategy implemented to access diphosphines with identical or different *P*-units.

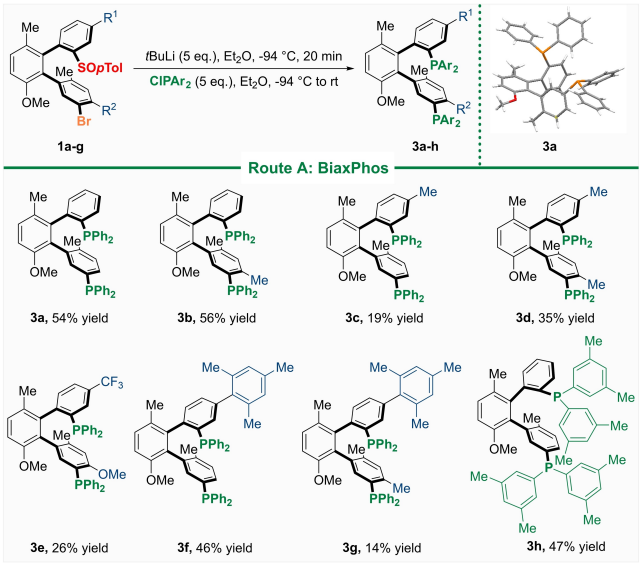

Scheme 3. Scope of diphosphines bearing the same phosphorus moiety.

conversion. The subsequent addition of chlorodiphenylphosphine (5 eq.) delivered the expected diphosphine **3a** in a good yield of 54%. Of note is that a low reaction temperature of −94 °C avoids the epimerization of the chiral axis and limits the undesired side reactions. This protocol was further used to build up a small library of BiaxPhos bearing two identical PAr_2 motifs. First, the backbone of the ligand was modified. The presence of an additional Me-substituent, at the R^1 position significantly decreased the efficiency of the reaction delivering ligand **3c** in 19% yield. This serious loss in reaction efficiency results from the low solubility of the corresponding precursor. In contrast, the presence of R^2-Me substituent on the other aromatic ring was beneficial for the reaction outcome as **3b** could be isolated in 56% yield. Interestingly, various substrates bearing both, R^1 and R^2 underwent smoothly the double lithium exchange, furnishing phosphines **3d** ($R^1 = R^2 = Me$), **3e** ($R^1 = CF_3$; $R^2 = Me$), **3f** (R^1 = mesityl; $R^2 = H$) or **3g** (R^1 = mesityl; $R^2 = Me$) bearing electronically and sterically diversified substituents in moderate to good yields. Finally, while using $P(3,5\text{-Me–Ph})_2Cl$ electrophile, this protocol could also be extended towards the synthesis of a more electron-rich and sterically hindered diphosphine **3h**.

In order to further extend the portfolio of new chiral phosphines and finely tune their steric and electronic properties, our further efforts focused on the chemoselective sequential functionalization of the *p*-tolylsulfinyl and Br-motifs (Scheme 2, Route B). The seminal work by Shi suggests that the rate of *p*-tolylsulfinyl/Mg exchange is in the same magnitude as iodine/Mg exchange, while Br/Mg exchange is expected to be 10^5

© 2023 The Authors. Advanced Synthesis & Catalysis published by Wiley-VCH GmbH

16154169, 2023, 12, Downloaded from https://onlinelibrary.wiley.com/doi/10.1002/adsc.202300527 by Universidad de la Rioja, Wiley Online Library on [29/11/2023]. See the Terms and Conditions (https://onlinelibrary.wiley.com/terms-and-conditions) on Wiley Online Library for rules of use; OA articles are governed by the applicable Creative Commons License

times slower.[13] Accordingly, by transposition with lithium bases and under finely optimized reaction conditions, chemoselective functionalization of the sulfoxide followed by the introduction of the second phosphine motif on the bromine position might be expected, although yet unprecedented in the literature.

At the outset of this study, **1a** was reacted with *t*BuLi (3 eq.) in toluene at −78 °C. The expected SO*p*Tol exchange was favored. However, double exchange could not be fully avoided, affording the expected monophosphine in 33% yield. Use of a weaker *n*BuLi base in combination with Et_2O/toluene medium furnished (see S.I., table 1) fully chemoselectively **2a** in 48% yield while avoiding epimerization issues (Scheme 4) and with the sole side product being the reduced product (removal of the sulfoxide motif). Surprisingly, the installation of the second phosphorus group has turned out to be highly challenging. While Br/Li exchange on monophosphine **2a** occurred smoothly in a presence of *t*BuLi, electrophilic trapping with PAr_2Cl was unproductive, delivering the reduced side product **4** (see S.I., table 2). Remarkably, the application of uncommon PAr_2OMe phosphinites as electrophiles turned out to be the solution of choice.[14] Indeed, in the presence of *t*BuLi and P(4-Me-C_6H_4)$_2$OMe at −94 °C, the monophosphine **2a** was converted smoothly into the corresponding diphosphine **3i** in excellent 86% yield. Under such finely optimized conditions, a small library of highly diverse BiaxPhos* bearing two different phosphorus moieties could be prepared in modest to excellent yields. The installation of the second phosphine unit is particularly efficient when electron-rich phosphinites are used and the reaction seems to tolerate well even sterically hindered phosphinite coupling partner (diphosphines **3j**–**3m**, or **3o**). Notably, *P*-chiral phosphinite is also a potent electrophile, affording an uncommon diphosphine ligand **3s** bearing three chirality elements, i.e., two atropisomeric axes together with a *P*-stereocenter. Unfortunately, the formation of the reduced products **4** cannot be fully avoided in some cases and the separation issues render the isolation of pure diphosphines **3l**, **3n** or **3q** difficult. In such cases, direct synthesis of metallic complexes may be envisioned, furnishing the pure bicoordinated P/P–Ir complexes.

Iridium-catalyzed asymmetric hydrogenation of imines

To explore the potential of these original ligands in asymmetric homogeneous catalysis, we have embarked on investigating asymmetric Ir-catalyzed imines hydro-

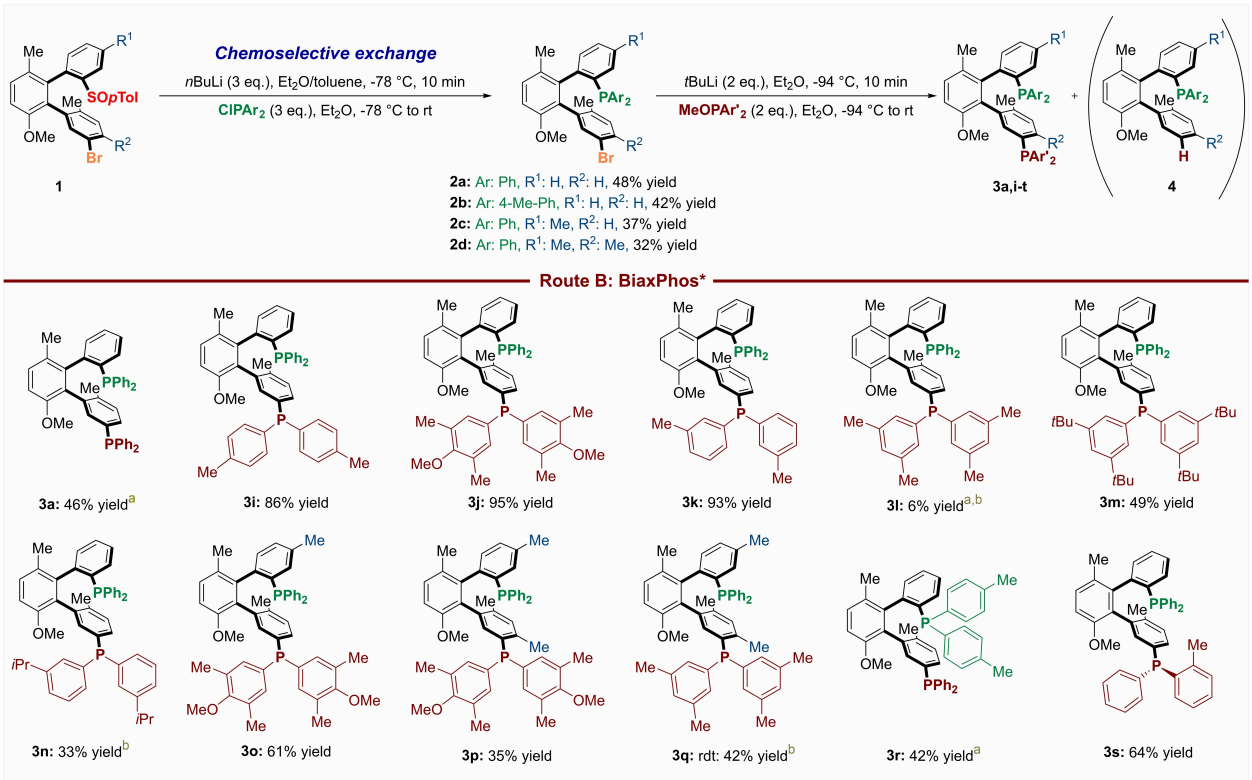

Scheme 4. Two-step synthesis of diphosphines BiaxPhos* with different phosphines via chemoselective reaction. a) *t*BuLi and phosphinite were added at −78 °C; b) Estimated yield as the product was obtained as an inseparable mixture with the reduced monophosphine **4**.

© 2023 The Authors. Advanced Synthesis & Catalysis published by Wiley-VCH GmbH

16154169, 2023, 12, Downloaded from https://onlinelibrary.wiley.com/doi/10.1002/adsc.202300527 by Universidad de la Rioja, Wiley Online Library on [29/11/2023]. See the Terms and Conditions (https://onlinelibrary.wiley.com/terms-and-conditions) on Wiley Online Library for rules of use; OA articles are governed by the applicable Creative Commons License

genation, an appealing transformation delivering enantiopure amines in a sustainable manner.[9]

To initiate this work, chiral Ir-BiaxPhos complexes were synthesized by reacting $[Ir(COD)Cl]_2$ and NaBArF with BiaxPhos ligands. The resulting complexes are stable, can be easily purified by silica gel column, and stored over several months under argon.

Hydrogenation of imine **5a**, selected as the benchmark substrate, was subsequently performed using chiral [Ir(COD)**3a**]BArF. Rapidly, we discovered that the reaction occurs smoothly in mesitylene under a low pressure of hydrogen, furnishing the amine **6a** in an enantiomeric ratio of 88:12 ((see S.I., Table 3), Table 1, entry 1). To further increase the chiral induction conferred by BiaxPhos, a catalyst screening was undertaken, focusing first on the steric hindrance and electronic properties of the phosphine moieties. Both, the electron-richness and the steric bulkiness of the phosphine motif on Ar^3 impact poorly the stereoinduction as the desired chiral amine was isolated in a rather constant enantiomeric ratio of 86:14 to 90:10, while reaching in all cases full substrate consumption within 3 h (Table 1, entries 2–5). In contrast, modification of the phosphine moiety on Ar^1 resulted in slight decrease in the reaction efficiency, furnishing **6a** in 85.5:14.5 er and 68% conversion (Table 1, entry 6).

Remarkably, modification of the chiral backbone significantly impacted the stereochemical outcome of the reaction. Introduction of the Me-substituents on either R^1 or R^2 positions increased the chiral induction up to 91.5:8.5 while a cumulative effect of both Me-substituents raised the enantiomeric ratio of the product up to 94:6 (Table 1, entries 7–9). Of note is that the presence of electron-withdrawing CF_3 substituent at R^1 significantly reduced the stereoselectivity of the reaction (Table 1, entry 10), while a racemic product was obtained when mesitylene-motif is introduced on the backbone, arguably due to a precluded coordination of the Ir with the proximal phosphine (Table 1, entry 11). Finally, the optimal results, i.e. er of 95:5 was obtained while combining the optimal chiral backbone and more sterically encumbered and more electron-rich phosphine group on Ar^3 (Table 1, entry 12).

With the optimized ligand **3q** in hand, the scope of the reaction was explored (Scheme 5). The hydrogenation occurs under mild conditions requesting a low catalyst loading (1 mol%) and total conversions are usually reached within 24 h while applying low H_2 over-pressure (1.5 bar). The reaction tolerates well various aromatic imines bearing a substituent in *para*-position, delivering the corresponding chiral benzylamines with excellent enantioselectivities, i.e. er $\geq$ 95:5 (**6a–e**). Extension of the aromatic substituent to a 2-naphthyl moiety resulted in the desired amine **6f** with er of 95:5 (Scheme 5). The best enantioselectivity ratio of 98.5:1.5 was reached with the imine **5g** featuring an easily removable *para*-methoxyphenyl group at the R'' position. It is also worth noting that the hydrogenation is chemoselective; the reduction of the C=N bond is observed selectively while challenging the reaction with substrates exhibiting an alkene or an alkyne motif (**6h**, **6i**, and **6j**). The imines bearing a

Table 1. Ligand optimization for the asymmetric hydrogenation of imines. a) er values were determined via high-performance liquid chromatography (HPLC) on a chiral stationary phase.

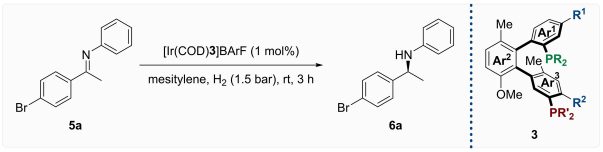

Entry	3	R	R'	R^1	R^2	conv (%)	er[a]	
1	**3a**	Ph	Ph	H	H	> 99	88:12	
2	**3j**	Ph	3,5-Me-4-MeO-Ph	-	-	> 99	88:12	
3	**3k**	Ph	3-Me-Ph	-	-	> 99	89:11	
4	**3l**	Ph	3,5-Me-Ph	-	-	> 99	90:10	Phosphines optimization
5	**3n**	Ph	3-*i*Pr-Ph	-	-	> 99	86:14	
6	**3r**	4-Me-Ph	Ph	-	-	68	85.5:14.5	
7	**3b**	Ph	Ph	H	Me	> 99	91.5:8.5	
8	**3c**	-	-	Me	H	> 99	91:9	
9	**3d**	-	-	Me	Me	> 99	94:6	Scaffold optimization
10	**3e**	-	-	CF_3	OMe	47	84.5:15.5	
11	**3g**	-	-	2,4,6-Me-Ph	Me	> 99	0	
12	**3q**	Ph	3,5-Me-Ph	Me	Me	> 99	95:5	

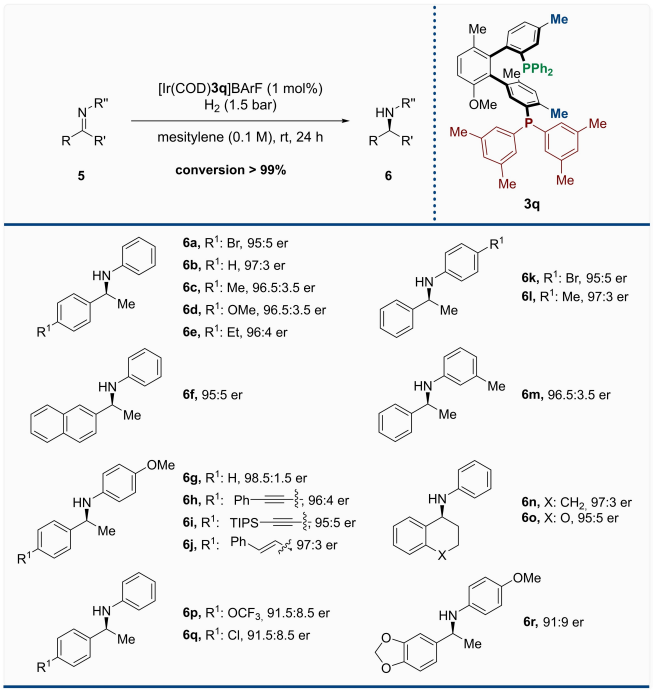

Scheme 5. Scope of chiral amines obtained by hydrogenation of imines catalyzed by an iridium-BiaxPhos* complex. All the products were obtained with the (*S*) stereochemistry according to the literature reference.

© 2023 The Authors. Advanced Synthesis & Catalysis published by Wiley-VCH GmbH

16154169, 2023, 12, Downloaded from https://onlinelibrary.wiley.com/doi/10.1002/adsc.202300527 by Universidad de la Rioja, Wiley Online Library on [29/11/2023]. See the Terms and Conditions (https://onlinelibrary.wiley.com/terms-and-conditions) on Wiley Online Library for rules of use; OA articles are governed by the applicable Creative Commons License

meta- or *para*- substitution on the R'' aromatic ring could be reduced with high enantioselectivities (**5k**, **5l**, and **5m**). Moreover, hydrogenation of **5n** and **5o** afforded the products with high optical purities. When imines bearing -OCF_3 or -Cl substituent in *para*-position, the amines **6p** and **6q** were delivered with slightly lower enantioselectivities. Enantioselectivity was also lower for the hydrogenation of **5r** bearing a benzodioxolane moiety. Reduction of more challenging substrates as azirines, hydrazones or *N*-alkyl imines was unsuccessful (Scheme S1). Finally, fifteen highly optically enantiopure amines could thus be prepared with excellent enantioselectivities $\geq$95:5 er and up to 98.5:1.5, revealing the remarkably potential of this ligand for the sustainable and mild synthesis of chiral amines.

Mechanistic study

Design of new ligands, featuring uncommon chirality pattern calls for the reinvestigation of the mechanism and determination of a stereomodel for a given transformation. Accordingly, to shed light on the catalytic activity of our ligands, we have initially endeavored the experimental mechanistic studies. First, as all attempts to crystalize Ir-BiaxPhos failed, NMR characterization of these complexes was performed. If coordination of the metal by both phosphines was evidenced in accordance with our hypothesis, a significant change in the ^{31}P NMR pattern was observed while comparing a standard Ir-BiaxPhos complex (Ir-**3a**) with Ir-**3d** complex, bearing methyl substituents on the R^2 position. Indeed, the presence of these additional substituents induced significant shift of the phosphorus peaks, and in particular presence of one signal at −104 ppm. This uncommon chemical displacement of the *P*-atom suggested the generation of a new species. To shed light into the complexation process, we analyzed the stability of [Ir(COD)**3d**]$^+$ via DFT calculations.[15] After optimizing the initial structure, starting from the X-ray of phosphine **3a** derivative,[16] we found that the C–H bond located in the biaryl moiety (Scheme 6, bottom) and the Ir-metal center are very close (2.68 Å). Interestingly, the direct activation of the C–H bond by the Ir metal center was accessible, with a free energy barrier of only 21.2 kcal/mol. An alternative C–H bond from the external aryl group was also explored but it was found both kinetically and thermodynamically unfavored (see Figure S11). The resulting cyclometalated species bearing a new Ir–H bond was found more stable than the initial complex by −1.6 kcal/mol. To further investigate this process, we calculated the NMR shift at the same level of theory of both the initial [Ir(COD)**3d**]$^+$ (Scheme 6, [Ir(I)]$^+$) and the resulting species after C–H bond activation (Scheme 6, [Ir(III)-H]$^+$). Interestingly, the difference in the calculated isotropic shift of both

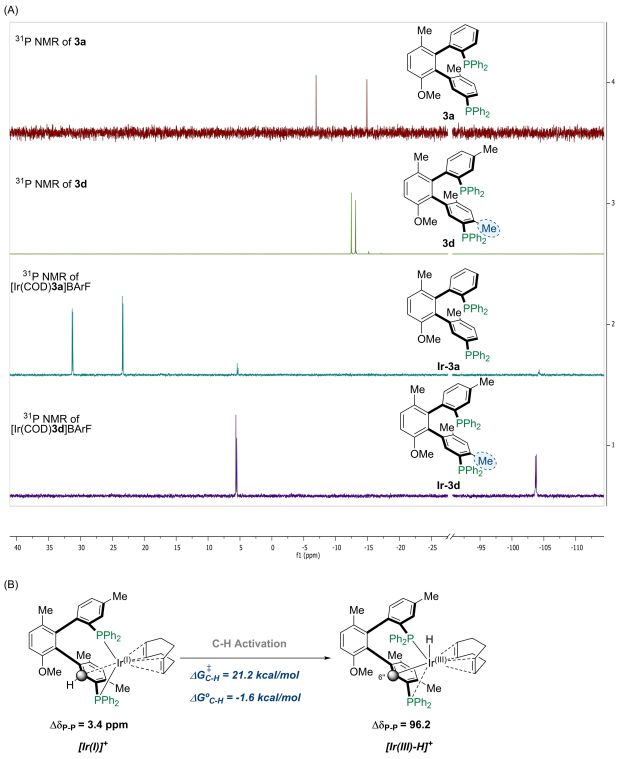

Scheme 6. (A) ^{31}P NMR of **3a**, **3d**, [Ir(COD)**3a**]BArF and [Ir(COD)**3d**]BArF; (B) Iridium(I) C–H activation of **3d**.

phosphines in [Ir(COD)**3d**]$^+$ is only 3.4 ppm, which is close to the difference observed in complex [Ir(COD)**3a**]$^+$. In contrast, the phosphorus NMR signals are largely displaced and separated after C–H activation process, showing a difference in the isotropic shift of both phosphorus centers of 96.2 ppm. Based on 2D phosphorus NMR, the clear shift of the signal can be attributed to the phosphine motif on the lower aromatic ring. This correlates very well with the experimental observation and suggest a stabilization of the [Ir(COD)**3d**] complex via C–H activation.

Subsequently, to investigate the mechanism of this transformation, the benchmark reaction was conducted under D_2 pressure (Scheme 7A). Surprisingly, the D-incorporation occurred not only on the expected benzylic carbon and nitrogen of substrates **5a** and **5b**. Under the standard reaction conditions, the introduction of 1 D atom was also observed on the CH_3 motifs, where one proton in total was fully exchanged with D. While imine **5a** was fully hydrogenated, conversion of substrate **5b** reached only 54% but full monodeuteration of the CH_3 motif was observed together with a partial deuteration at the *ortho*-position. In the same line, while using imine substrate **5s** featuring CD_3 methylene motif, hydrogenation under H_2 pressure also led to the introduction of approximately 1 H-atom in total on the CD_3 unit (Scheme 7B). These observations suggest the addition of one atom (either H or D,

© 2023 The Authors. Advanced Synthesis & Catalysis published by Wiley-VCH GmbH

16154169, 2023, 12, Downloaded from https://onlinelibrary.wiley.com/doi/10.1002/adsc.202300527 by Universidad de la Rioja, Wiley Online Library on [29/11/2023]. See the Terms and Conditions (https://onlinelibrary.wiley.com/terms-and-conditions) on Wiley Online Library for rules of use; OA articles are governed by the applicable Creative Commons License

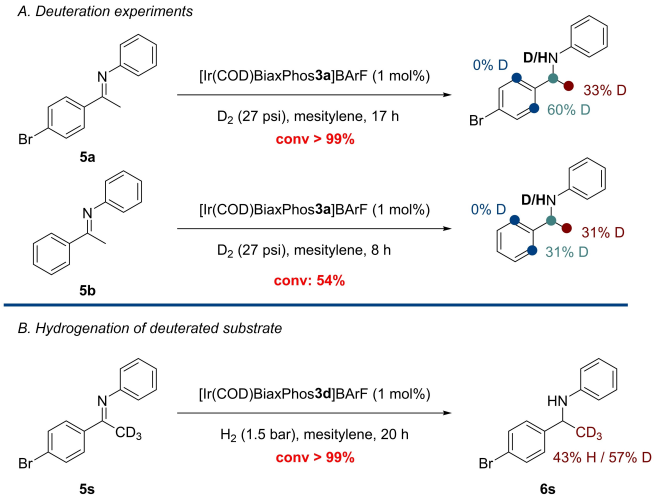

Scheme 7. Reduction of **5a** and **5b** under D_2 pressure; reduction of the deuterated substrate **5s** under H_2.

depending of the gas used) on the alpha position of the C=N bond, and subsequently that enamine tautomer might play a crucial role in the mechanism of this transformation. This result is extremely interesting, suggesting that an alternative mechanism might be operating for this asymmetric hydrogenation with BiaxPhos-type ligands compared to the literature known catalytic cycles involving either inner- or outer-sphere imine's hydrogenation pathway.

Considering the unexpected experimental results indicating enamine generation during our reaction, detailed DFT calculations[35] have been conducted to 1) define the catalytically active Ir-catalyst; 2) elucidate the mechanism of this transformation and 3) the nature of the enantioselectivity determining step occurring either from the imine or the enamine tautomers.[17]

As a preliminary work, the stability of the corresponding enamine/imine tautomerization process was evaluated. It is well-established that both tautomers coexist in solution although the higher stability of the imine (7.6 kcal/mol more stable) implies that the equilibrium is strongly displaced towards the imine tautomer. However, during the catalytic cycle, activation of the enamine by Ir(III) is also accessible due to the more activated character of the C=C bond (*vide infra*).

Second key question concerns the nature of the catalytically active Ir-BiaxPhos catalyst. Indeed, although the cyclometallated Ir(III)-H complex seems to be a major species, catalytic activity of this complex might be questioned. Low temperature ^1H and ^{31}P NMR experiments showed that iridium hydride species [Ir(COD)**3d**], may be unable to activate H_2 molecules. Furthermore, this complex is in equilibrium with the non cyclometallated Ir(I)-BiaxPhos complex as evidenced by a ^{31}P NMR spectrum performed at 215 K (See Figure S8). It can be thus speculated that the cationic Ir(I)-BiaxPhos is the catalytic active species. To confirm this hypothesis by DFT calculations, the speciation of the catalyst under H_2 atmosphere was computed (See Figure S12). As expected, COD ligand can be easily hydrogenated and an Ir(III) species is formed upon addition of a H_2 molecule to Ir(I) center. This process is downhill by 12.4 kcal/mol and forms $\mathbf{[Ir(III)\text{-}(H)_2]^+}$ complex. From here, we explored a second H_2 coordination, which is exergonic by 6.4 kcal/mol and leads to the most stable species found ($\mathbf{[Ir(III)\text{-}(H)_2H_2]^+}$). In order to discard Ir(V) as the reactive center, we also explored the H–H bond breaking event from this activated catalyst but it was endergonic by 9.3 kcal/mol, suggesting that the participation of Ir(V) in the mechanism is unlikely due to the low barriers found in the Ir(III) mechanisms (see below). Thus, $\mathbf{[Ir(III)\text{-}(H)_2H_2]^+}$ was set as the reference point to explore three possible reaction mechanisms:[10b,18] A) an outer sphere imine hydrogenation, B) Ir(III)/Ir(I) inner sphere imine hydrogenation and Ir(III) H_2 assisted imine hydrogenation. Those mechanisms were complemented by C) the inner sphere Ir(III)/Ir(I) and Ir(III) H_2 hydrogenation of enamine, as suggested by the deuteration experiments commented above.

We began our analysis by exploring the outer-sphere imine hydrogenation mechanism A (Scheme 8), which is one of the most accepted pathways in the bibliography.[18] Initially, the basic nitrogen from the imine moiety can split the H–H bond of the coordi-

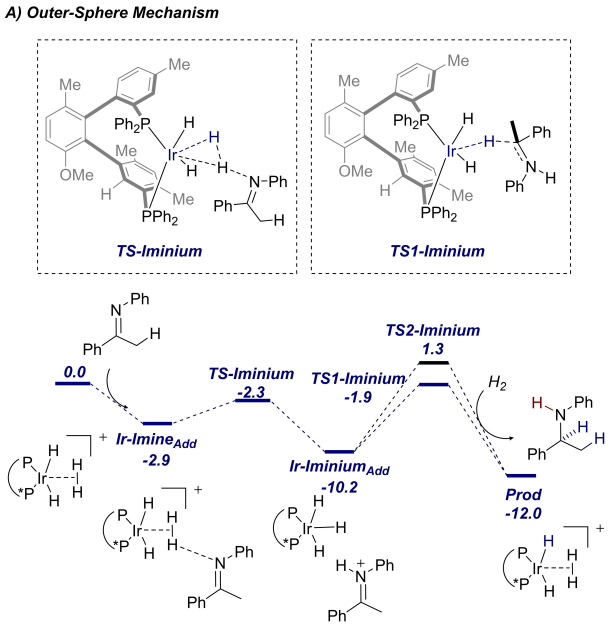

Scheme 8. Free energy profile of outer-sphere imine hydrogenation mechanism (A) for both enantiomers. Energies in kcal/mol.

© 2023 The Authors. Advanced Synthesis & Catalysis published by Wiley-VCH GmbH

16154169, 2023, 12, Downloaded from https://onlinelibrary.wiley.com/doi/10.1002/adsc.202300527 by Universidad de la Rioja, Wiley Online Library on [29/11/2023]. See the Terms and Conditions (https://onlinelibrary.wiley.com/terms-and-conditions) on Wiley Online Library for rules of use; OA articles are governed by the applicable Creative Commons License

nated H_2 forming exergonically the iminium ion and the corresponding neutral L–IrH_3 species. This process is almost barrierless (0.6 kcal/mol), accessible at the reaction temperature. From that point, hydride transfer from the catalyst to the highly electrophilic carbon of the iminium moiety might take place from the two different faces of the iminium ion to form the two product enantiomers. As expected, the experimental major *S* enantiomer is generated through a lower barrier transition state **TS1-Iminium** (8.3 kcal/mol) compared to the minor enantiomer (11.5 kcal/mol). Although this mechanism is feasible, the deuteration experiment suggested that outer-sphere pathway is unlikely, so we explored other alternatives.

Then we proceed with the exploration of the imine/enamine hydrogenation through the inner sphere mechanisms (Scheme 9), i.e. possibilities B and C. In this case, an Ir(III)/Ir(I) mechanism (Scheme 9, top) and an Ir(III)-H_2 assisted mechanism (Scheme 9, bottom) were explored. As it is shown in Scheme 9B, the initial step corresponds to the insertion of the metal into the C=C bond of the enamine. This step is stereoselective as the configuration of the *C*-stereogenic center is fixed. Accordingly, this initial insertion of the Ir–H bond into the α position enamine tautomer is slightly favored in **TS1** (generating the major *S*-product) as respect to the transition state that yields to the opposite enantiomer intermediate (**TS2**). This first step shows also that the expected enamine hydrogenation is energetically favored (−2.8 kcal/mol) over the imine reduction (−1.1 kcal/mol). It was worth to note that insertion into the β-position of the enamine was found to be more energetic (see Figure S13 in the Supporting Information).

The resulting intermediates were higher in energy than the initial imine so this step does not determine the enantioselectivity. Furthermore, direct inner-sphere imine protonation followed by hydride transfer was found not possible as the intermediate always reversed to the initial **Add3-4** species from the imine. Then, we analyzed the final reductive elimination to yield the hydrogenated product in both enamine and imine pathways. This second step is accessible in the enamine pathway, with an overall free energy barrier of 24.2 kcal/mol for the experimentally observed *S*-enantiomer (**TS1'**) and corresponds to a predicted enantiomeric ratio of 95:5 in close agreement with the experimental value (97:3). The enantiomeric transition state **TS2'** is 1.78 kcal/mol higher in energy. In contrast, the reductive elimination between the hydride and the *N* of the imine pathways is highly energetic and not accessible under reaction conditions (**TS3'** and **TS4'**). This enamine hydrogenation pathway B proceeding through an Ir(III)/Ir(I) mechanism is also competitive when compared to the H_2 assisted mechanism C (Scheme 9 bottom), where a final reductive elimination step forming Ir(I) is prevented. In that case, after the initial H migration due to the presence of a vacancy in the Ir coordination sphere, H_2 coordinates the Ir(III) species to form the corresponding **Int(1-4)-H_2** adducts. From here, the final protonation of the nitrogen atom (**TS3'-H_2** in the imine pathway) or the β-carbon (**TS1'-H_2** in the enamine pathway) occurs through the concerted breaking of the coordinated H_2 ligand, regenerating the initial catalyst and forming the final product. The enamine hydrogenation pathway C is slightly more favorable than pathway A for the formation of the minor (*R*) enantiomer and it describes properly the experimentally observed (*S*) enantioselectivity as opposed to the assisted imine hydrogenation which is requiring much more energy especially for the elimination step. Finally, it was worth to note the initial insertion of the enamine into Ir–H bond of catalyst **$[Ir(III)\text{-}(H)_2H_2]^+$** was also explored in order to check the formation of Ir(V) as an alternative pathway but it was found not feasible due to the sterically hindered Ir center (see Figure S14).

Overall, the free energy span of the inner sphere mechanisms B and C implying an enamine and the outer-sphere mechanism A involving an iminium are very close in energy (24.2 kcal/mol, 24.0 kcal/mol and 23.7 kcal/mol respectively) and can compete under reaction conditions. Interestingly, Ir(III)/Ir(I) and Ir(III)-H_2 assisted mechanism for enamine hydrogenation can operate under our reaction conditions whereas direct hydrogenation of the imine species under inner-sphere pathways is virtually impossible (free energy barriers of 44.6 kcal/mol for B and 43.4 kcal/mol for C). The energy profiles calculated for the pathways B and C also coherent with the deuteration observed at the β-carbon of the enamine, although deuteration through tautomerization cannot be excluded due to competition of an outer sphere mechanism. As a final remark, the chiral ligand favors the formation of the (*S*) enantiomer in all the reaction pathways explored.

Accordingly, based on the experimental investigations, in-operando studies and DFT calculations, an unprecedented catalytic cycle for the asymmetric Ir-BiaxPhos* catalyzed imine hydrogenation can be proposed (Scheme 10). This catalytic cycle starts with the coordination of the enamine tautomer to Ir(III) species formed *in situ* by hydrogenation of the Ir(I) precursor. Then, the enantioselective insertion of the C–C double bond into Ir–H bond generates stereoselectively the tertiary (*S*)-carbon and a carbanion coordinated to the Ir(III) intermediate. Finally, a reductive elimination or a hydrogen assisted elimination releases the hydrogenated product and regenerates the catalyst.

© 2023 The Authors. Advanced Synthesis & Catalysis published by Wiley-VCH GmbH

16154169, 2023, 12, Downloaded from https://onlinelibrary.wiley.com/doi/10.1002/adsc.202300527 by Universidad de la Rioja, Wiley Online Library on [29/11/2023]. See the Terms and Conditions (https://onlinelibrary.wiley.com/terms-and-conditions) on Wiley Online Library for rules of use; OA articles are governed by the applicable Creative Commons License

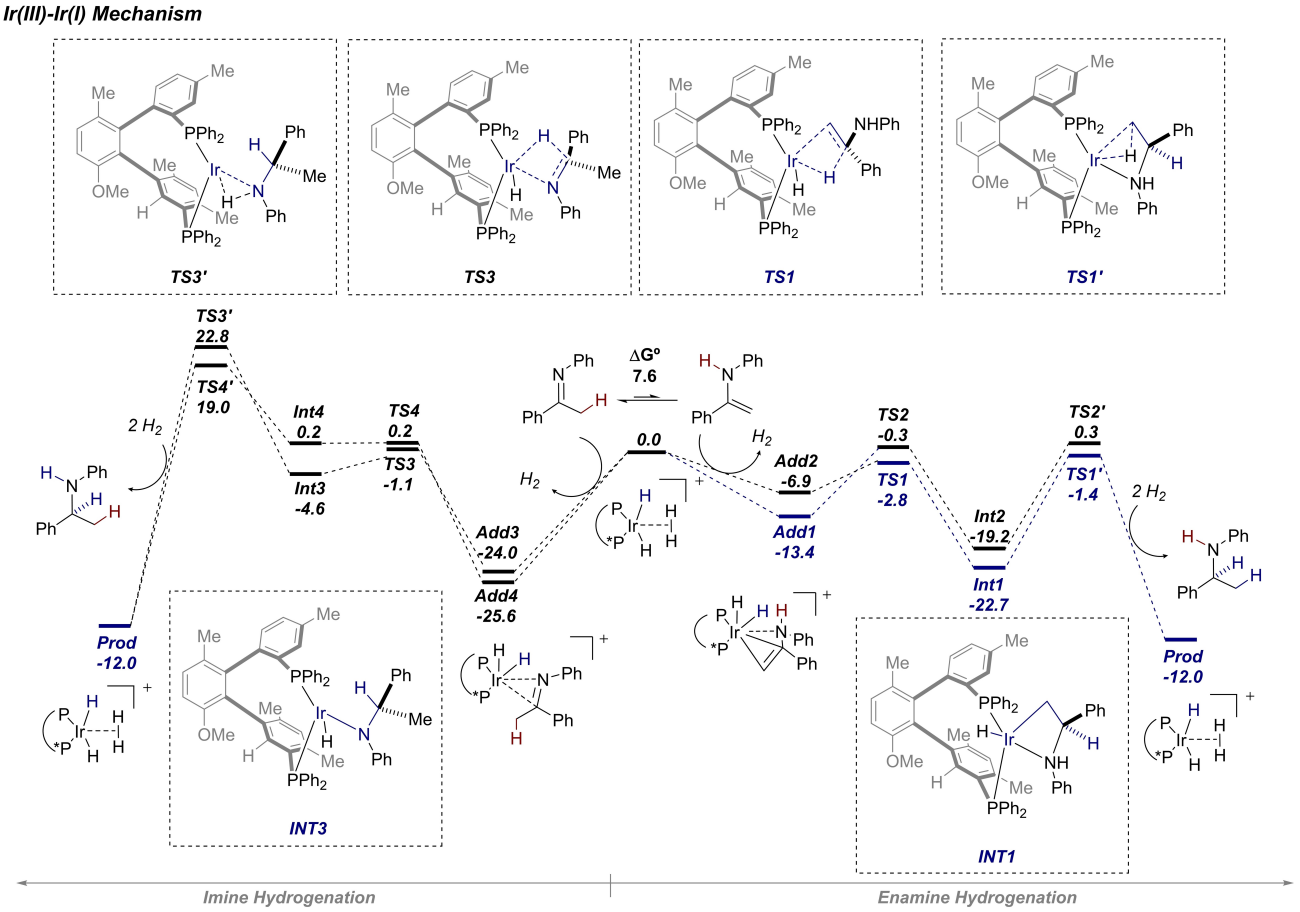

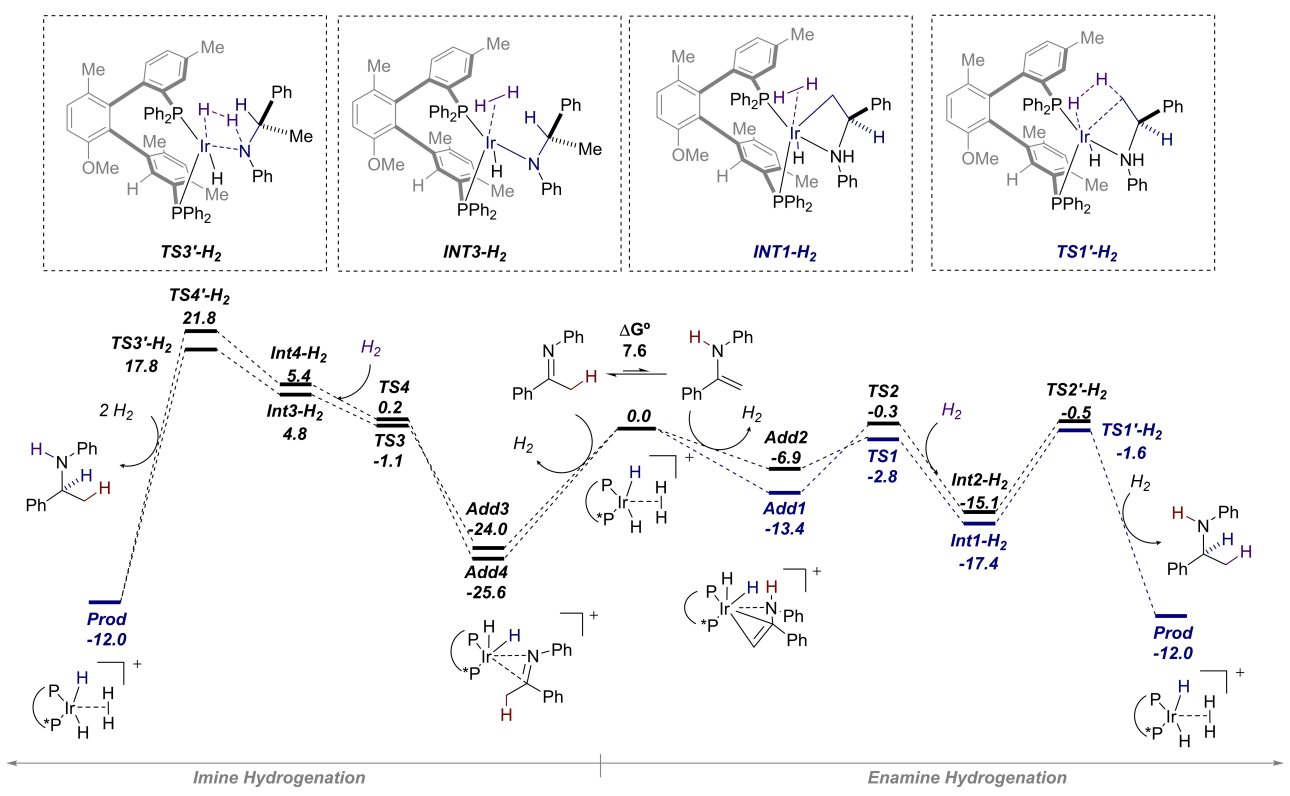

Scheme 9. Free energy profiles of enamine vs imine hydrogenation catalyzed by Ir complex. Energies in kcal/mol.

© 2023 The Authors. Advanced Synthesis & Catalysis published by Wiley-VCH GmbH

16154169, 2023, 12, Downloaded from https://onlinelibrary.wiley.com/doi/10.1002/adsc.202300527 by Universidad de la Rioja, Wiley Online Library on [29/11/2023]. See the Terms and Conditions (https://onlinelibrary.wiley.com/terms-and-conditions) on Wiley Online Library for rules of use; OA articles are governed by the applicable Creative Commons License

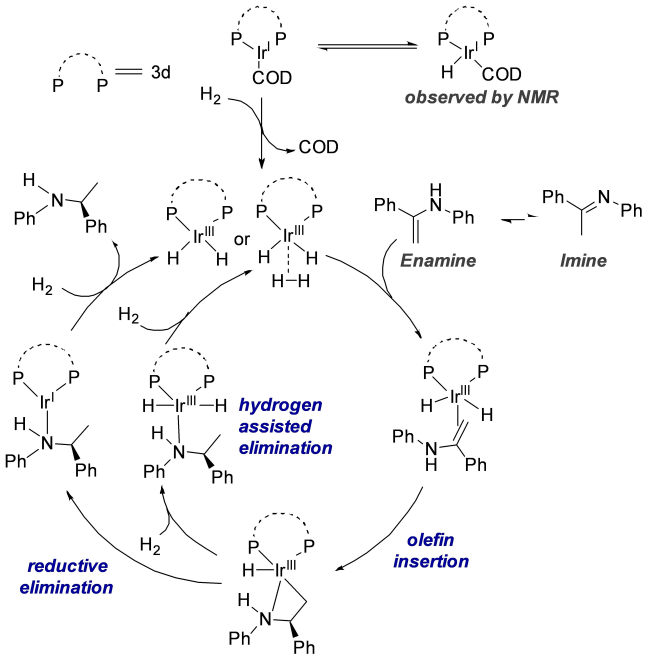

Scheme 10. Simplified catalytic cycle.

Conclusion

In conclusion, we report herein a new entry towards the synthesis of fully modulable, chiral C_1-symmetric diphosphines, bearing two distinguished coordinating motifs. Their synthesis via late-stage modification of an advanced enantiopure scaffolds provides a unique opportunity to rapidly access a large library of ligands from a common precursor. Thus, designed new ligands turned out to be highly appealing for challenging asymmetric imine hydrogenation, operating under mild reaction conditions and near to atmospheric pressure of H_2. Remarkably, combined experimental investigations and DFT calculations highlighted a unique mode of action of the corresponding Ir-BiaxPhos complexes, promoting the imine reduction via an original mechanism involving initial enamine generation.

Experimental Section

General procedure for the synthesis of BiaxPhos ligands: A solution of **1** (1 eq.) in Et_2O (0.1 M) was cooled to −94 °C. A solution of *t*BuLi (5 eq., 1.7 M in pentane) was then added dropwise (color changed to dark brown). The resulting mixture was stirred at −94 °C for 20 min, when a solution of $ClPAr_2$ (5 eq.) in Et_2O (1 M) was slowly cannulated. The resulting mixture was stirred until it warmed to room temperature and was quenched by filtration over a silica gel pad (washed with Et_2O, some DCM can be added to solubilize the reaction mixture before). Solvent was removed under reduced pressure, and flash chromatography (Et_2O /*n*-pentane 10:90, product loaded as 20:80 DCM/*n*-pentane solution) afforded the diphosphine **3**.

General procedure for the synthesis of dissymmetrical BiaxPhos* ligands:

Step1: To a solution of (1′*S*,2′*R*)-5-bromo-6′-methoxy-2,3′-dimethyl-2″-((*S*)-*p*- tolylsulfinyl)-1,1′:2′,1″-terphenyl **1 a** (1 eq., 290 mg, 0.574 mmol) in toluene (5 mL) at −78 °C in a Schlenk under argon, was added dropwise *n*BuLi (3.35 eq., 1.6 M, 1.2 mL, 1.92 mmol). The mixture was stirred 2 min then Et_2O (1 mL) cooled down to −78 °C was added and the solution was stirred 5 min at − 78 °C. A solution of $ClPAr_2$ (3.4 eq., 430 mg, 0.35 mL, 1.95 mmol) in Et_2O (0.4 mL) was then added dropwise and stirred 15 min at −78 °C, then allowed to come back at 0 °C when the cooling bath was removed. The mixture was diluted with Et_2O and filtered on silica plug with Et_2O. The solution was concentrated and purified by chromatography on silica gel with argon flow (Et_2O/*n*-pentane 5:95, product loaded as 20:80 DCM/*n*-pentane solution) to afford the ((1′*R*,2′*S*)-5″-bromo-3′-methoxy-2″,6′-dimethyl-[1,1′:2′,1″-terphenyl]-2-yl)diphenylphosphane **2 a** as a white powder (152 mg, 0.276 mmol, **48%** yield).

Step 2: A solution of **1** (1 eq.) in Et_2O (0.1 M) was cooled to −94 °C. A solution of *t*BuLi (5 eq., 1.7 M in pentane) was then added dropwise (color changed to dark brown). The resulting mixture was stirred at −94 °C for 20 min, when a solution of $ClPAr_2$ (5 eq.) in Et_2O (1 M) was slowly cannulated. The resulting mixture was stirred until it warmed to room temperature and was quenched by filtration over a silica gel pad (washed with Et_2O, some DCM can be added to solubilize the reaction mixture before). Solvent was removed under reduced pressure, and flash chromatography (Et_2O /*n*-pentane 10:90, product loaded as 20:80 DCM/*n*-pentane solution) afforded the diphosphine **3**.

General procedure for the synthesis of Ir-complexes: In a Schlenk under argon, the bis(1,5-cyclooctadiene)diiridium(I) dichloride (1 eq.) and the $NaBAr_F$ (2.2 eq.) are dissolved in anhydrous DCM (0.02 M) and then the 1,5-cyclooctadiene (140 eq.) is added dropwise. The reaction is stirred for 30 min and a solution of BiaxPhos **3** (2.2 eq.) in anhydrous DCM (0.02 M) is added dropwise. The color turned from dark purple to red. The reaction is stirred one hour at room temperature and then concentrated under high vacuum. The red oil is purified by column chromatography on silica gel with cyclohexane:DCM (1:0 to 1:1) as eluent and with argon flow. The red oil obtained is concentrated at 50 °C overnight under high vacuum to obtain the product as a deep red powder or an orange foam.

General procedure for imine hydrogenation: In the glove box, the imine 5 (20 mg) and the complex [Ir(COD)3q]BArF (1 mol%) are placed in a vial. Then, the vial is removed from the glove box and then anhydrous mesitylene (0.1 M) is added. The reaction mixture is put into the autoclave and the system is purged with hydrogen at 1.5 bar 3 times. The hydrogen pressure is adjusted to 1.5 bar and the reaction is stirred at room temperature for 24 h. After careful hydrogen release, the solution is filtrated over a celite plug (eluting with DCM) and concentrated to afford the pure amine. Purification by chromatography on silica gel (c-Hex/EtOAc as eluent) can be performed if required

© 2023 The Authors. Advanced Synthesis & Catalysis published by Wiley-VCH GmbH

16154169, 2023, 12, Downloaded from https://onlinelibrary.wiley.com/doi/10.1002/adsc.202300527 by Universidad de la Rioja, Wiley Online Library on [29/11/2023]. See the Terms and Conditions (https://onlinelibrary.wiley.com/terms-and-conditions) on Wiley Online Library for rules of use; OA articles are governed by the applicable Creative Commons License

Acknowledgements

We thank the CNRS (Centre National de la Recherche Scientifique), the "Ministere de l'Education Nationale et de la Recherche", France, for financial support. G.H. and Q.D. are very grateful to the "ministère de l'Education Nationale et de la Recherche", France for a doctoral grant. R.A.A.A. acknowledges CNRS for postdoctoral funding with project "CNRS INC Prematuration". We acknowledge Pr. Sylvain Jugé from Université de Bourgogne-Franche-Comté, France, for the generous gift of a P-stereogenic precursor. I.F.-A acknowledge the University of La Rioja for financial support and "Beronia" high performing computing center for computational resources and Spanish Ministry MICINN for financial support (IJC2020-045125-I).

References

[1] T. P. Dang, H. B. Kagan, *J. Chem. Soc. Chem. Commun.* **1971**, *10*, 481.

[2] a) W. Tang, X. Zhang, *Chem. Rev.* **2003**, *103*, 3029–3070; b) K. Aikawa, K. Mikami, *Chem. Commun.* **2012**, *48*, 11050; c) T. P. Yoon, E. N. Jacobsen, *Science* **2003**, *299*, 1691–1693; d) J.-H. Xie, Q.-L. Zhou, *Acc. Chem. Res.* **2008**, *41*, 581–593; e) C. Li, F. Wan, Y. Chen, H. Peng, W. Tang, S. Yu, J. C. McWilliams, J. Mustakis, L. Samp, R. J. Maguire, *Angew. Chem. Int. Ed.* **2019**, *58*, 13573–13583.

[3] a) K. Achiwa, *J. Am. Chem. Soc.* **1976**, *98*, 8265–8266; b) A. Gavryushin, K. Polborn, P. Knochel, *Tetrahedron: Asymmetry* **2004**, *15*, 2279–2288.

[4] A. Togni, C. Breutel, A. Schnyder, F. Spindler, H. Landert, A. Tijani, *J. Am. Chem. Soc.* **1994**, *116*, 4062–4066.

[5] T. Sturm, W. Weissensteiner, F. Spindler, *Adv. Synth. Catal.* **2003**, *345*, 160–164.

[6] a) W. Chen, F. Spindler, B. Pugin, U. Nettekoven, *Angew. Chem. Int. Ed.* **2013**, *52*, 8652–8656; b) C. Chen, H. Wang, Z. Zhang, S. Jin, S. Wen, J. Ji, L. W. Chung, X.-Q. Dong, X. Zhang, *Chem. Sci.* **2016**, *7*, 6669–6673.

[7] a) Q. Dherbassy, G. Schwertz, M. Chessé, C. K. Hazra, J. Wencel-Delord, F. Colobert, *Chem. Eur. J.* **2016**, *22*, 1735–1743; b) C. K. Hazra, Q. Dherbassy, J. Wencel-Delord, F. Colobert, *Angew. Chem. Int. Ed.* **2014**, *53*, 13871–13875; c) S. Jerhaoui, F. Chahdoura, C. Rose, J.-P. Djukic, J. Wencel-Delord, F. Colobert, *Chem. Eur. J.* **2016**, *22*, 17397–17406; d) S. Jerhaoui, J.-P. Djukic, J. Wencel-Delord, F. Colobert, *Chem. Eur. J.* **2017**, *23*, 15594–15600.

[8] Q. Dherbassy, J.-P. Djukic, J. Wencel-Delord, F. Colobert, *Angew. Chem. Int. Ed.* **2018**, *57*, 4668–4672.

[9] a) N. Fleury-Brégeot, V. de la Fuente, S. Castillón, C. Claver, *ChemCatChem* **2010**, *2*, 1346–1371; b) J.-H. Xie, S.-F. Zhu, Q.-L. Zhou, *Chem. Rev.* **2011**, *111*, 1713–1760; c) W. Li, X. Zhang, in *Stereoselective Formation of Amines* (Eds.: W. Li, X. Zhang), Springer Berlin Heidelberg, Berlin, Heidelberg, **2013**, pp. 103–144; d) K. H. Hopmann, A. Bayer, *Coord. Chem. Rev.* **2014**, *268*, 59–82; e) R. A. A. Abdine, G. Hedouin, F. Colobert, J. Wencel-Delord, *ACS Catal.* **2021**, *11*, 215–247; f) M. Diéguez, C. Claver, J. Margalef, in *Advances in Catalysis* (Eds.: M. Diéguez, A. Pizzano), Academic Press, **2021**, pp. 205–289; g) J. Barrios-Rivera, Y. Xu, M. Wills, V. K. Vyas, *Org. Chem. Front.* **2020**, *7*, 3312–3342; h) D. Zhao, L. Candish, D. Paul, F. Glorius, *ACS Catal.* **2016**, *6*, 5978–5988.

[10] a) X. Wei, B. Qu, X. Zeng, J. Savoie, K. R. Fandrick, J.-N. Desrosiers, S. Tcyrulnikov, M. A. Marsini, F. G. Buono, Z. Li, B.-S. Yang, W. Tang, N. Haddad, O. Gutierrez, J. Wang, H. Lee, S. Ma, S. Campbell, J. C. Lorenz, M. Eckhardt, F. Himmelsbach, S. Peters, N. D. Patel, Z. Tan, N. K. Yee, J. J. Song, F. Roschangar, M. C. Kozlowski, C. H. Senanayake, *J. Am. Chem. Soc.* **2016**, *138*, 15473–15481; b) K. H. Hopmann, A. Bayer, *Organometallics* **2011**, *30*, 2483–2497; c) B. Tutkowski, S. Kerdphon, E. Limé, P. Helquist, P. G. Andersson, O. Wiest, P.-O. Norrby, *ACS Catal.* **2018**, *8*, 615–623.

[11] a) O. Riant, G. Argouarch, D. Guillaneux, O. Samuel, H. B. Kagan, *J. Org. Chem.* **1998**, *63*, 3511–3514; b) P. B. Hitchcock, G. J. Rowlands, R. Parmar, *Chem. Commun.* **2005**, 4219; c) F. R. Leroux, A. Berthelot, L. Bonnafoux, A. Panossian, F. Colobert, *Chem. Eur. J.* **2012**, *18*, 14232–14236.

[12] N. Furukawa, S. Ogawa, K. Matsumura, H. Fujihara, *J. Org. Chem.* **1991**, *56*, 6341–6348.

[13] L. Shi, Y. Chu, P. Knochel, H. Mayr, *Org. Lett.* **2012**, *14*, 2602–2605.

[14] J. Bayardon, Y. Rousselin, S. Jugé, *Org. Lett.* **2016**, *18*, 2930–2933.

[15] Calculations were carried out at CPCM(Mesitylene) ωB97xD/6-311++G(3d,2p)/LANL2TZ(f)(Ir)//ωB97xD/6-31G(d)/LANL2DZ (for Ir) (See Supporting Information for Computational Details and benchmarking study).

[16] Deposition numbers 2160082 (for **3a**) contain the supplementary crystallographic data for this paper. These data are provided free of charge by the joint Cambridge Crystallographic Data Centre and Fachinformationszentrum Karlsruhe Access Structures service.

[17] a) X. Jie, Y. Shang, Z.-N. Chen, X. Zhang, W. Zhuang, W. Su, *Nat. Commun.* **2018**, *9*, 5002; b) J. H. Babler, M. C. Atwood, J. E. Freaney, A. R. Viszlay, *Tetrahedron Lett.* **2007**, *48*, 7665–7667; c) L. O. Davis, M. A. Putri, C. L. Meyer, C. P. Durant, *Tetrahedron Lett.* **2014**, *55*, 3100–3103; d) Y. Wei, I. Deb, N. Yoshikai, *J. Am. Chem. Soc.* **2012**, *134*, 9098–9101.

[18] a) G. E. Dobereiner, A. Nova, N. D. Schley, N. Hazari, S. J. Miller, O. Eisenstein, R. H. Crabtree, *J. Am. Chem. Soc.* **2011**, *133*, 7547–7562; b) M. Sparta, C. Riplinger, F. Neese, *J. Chem. Theory Comput.* **2014**, *10*, 1099–1108.

© 2023 The Authors. Advanced Synthesis & Catalysis published by Wiley-VCH GmbH

16154169, 2023, 12, Downloaded from https://onlinelibrary.wiley.com/doi/10.1002/adsc.202300527 by Universidad de la Rioja, Wiley Online Library on [29/11/2023]. See the Terms and Conditions (https://onlinelibrary.wiley.com/terms-and-conditions) on Wiley Online Library for rules of use; OA articles are governed by the applicable Creative Commons License